Dwarf galaxies in the Coma cluster – I. Velocity dispersion measurements⋆†

E. Kourkchi,[1,2]‡ H. G. Khosroshahi,[1] D. Carter,[3] A. M. Karick,[3] E. Mármol-Queraltó,[4]
K. Chiboucas,[5,6] R. B. Tully,[5] B. Mobasher,[7] R. Guzmán,[8] A. Matković[9]
and N. Gruel[10]

[1]*School of Astronomy, Institute for Research in Fundamental Sciences (IPM), PO Box 19395-5531, Tehran, Iran*
[2]*Department of Physics, Sharif University of Technology, PO Box 11155-9161, Tehran, Iran*
[3]*Astrophysics Research Institute, Liverpool John Moores University, Twelve Quays House, Egerton Wharf, Birkenhead CH41 1LD*
[4]*Departamento de Astrofísica, Facultad de Ciencias Físicas, Universidad Complutense de Madrid, 28040 Madrid, Spain*
[5]*Institute for Astronomy, University of Hawaii, 2680 Woodlawn Drive, Honolulu, HI 96821, USA*
[6]*Gemini Observatory, Northern Operations Center, 670 N. A'ohoku Place, Hilo, HI 96720, USA*
[7]*Department of Physics and Astronomy, University of California, Riverside, CA 92521, USA*
[8]*Department of Astronomy, University of Florida, PO Box 112055, Gainsville, FL 32611-2055, USA*
[9]*Department of Astronomy and Astrophysics, Pennsylvania State University, University Park, PA 16802, USA*
[10]*Centro de Estudios de Física del Cosmos de Aragón, C. General Pizarro, 1-3 44001 Teruel, Spain*

ABSTRACT

We present the study of a large sample of early-type dwarf galaxies in the Coma cluster observed with DEIMOS on the Keck II to determine their internal velocity dispersion. We focus on a subsample of 41 member dwarf elliptical galaxies for which the velocity dispersion can be reliably measured, 26 of which were studied for the first time. The magnitude range of our sample is $-21 < M_R < -15$ mag.

This paper (Paper I) focuses on the measurement of the velocity dispersion and their error estimates. The measurements were performed using penalized pixel fitting (PPXF) and using the calcium triplet absorption lines. We use Monte Carlo bootstrapping to study various sources of uncertainty in our measurements, namely statistical uncertainty, template mismatch and other systematics. We find that the main source of uncertainty is the template mismatch effect which is reduced by using templates with a range of spectral types.

Combining our measurements with those from the literature, we study the Faber–Jackson relation ($L \propto \sigma^\alpha$) and find that the slope of the relation is $\alpha = 1.99 \pm 0.14$ for galaxies brighter than $M_R \simeq -16$ mag. A comprehensive analysis of the results combined with the photometric properties of these galaxies is reported in Paper II.

Key words: galaxies: clusters: individual: Coma – galaxies: dwarf – galaxies: elliptical and lenticular, cD – galaxies: evolution – galaxies: fundamental parameters – galaxies: kinematics and dynamics.

1 INTRODUCTION

A clear understanding of dwarf galaxies and their relation to their most massive counterparts is essential for testing galaxy formation models. Although the lowest luminosity dwarf galaxies ($M_v \sim -9$) appear to contain large amounts of dark matter (Aaronson 1983; Mateo 1998), for brighter dwarfs the situation is less clear. De Rijcke et al. (2006) find that the dwarf companions to M31, at $M_v \sim -14$, contain around 40–50 per cent dark matter by mass within the inner two half-light radii. Geha, Guhathakurta & van der Marel (2002) find that six Virgo cluster dwarfs at $M_v \sim -16$ do not show evidence for dark matter within an effective radius. Toloba et al. (2011) observe a larger sample of Virgo dwarfs and again find that

they are not dark matter dominated. Here we observe a sample of Coma cluster dwarfs in a somewhat brighter magnitude range ($21 < M_R < 15$) in order to understand better their internal dynamics. Our goals are the extension of the Faber–Jackson (FJ) relation ($L \propto \sigma^\alpha$) and the Fundamental Plane (Djorgovski & Davis 1987; Dressler et al. 1987; Bender, Burstein & Faber 1992) relating luminosity, velocity dispersion, surface brightness and scale length of galaxies to the low-luminosity dwarf population, providing important tools for studying formation of galaxies. For example, the precise value of the exponent of the FJ relation, α, helps to constrain galaxy formation models as it is sensitive to the effect of gas loss from self-gravitating systems (Dekel & Silk 1986; Yoshii & Arimoto 1987). In the case where a dark matter halo governs the galaxy dynamics, α is predicted to be 5.26 and $M/L \propto L^{0.37}$. If, instead, the galaxies contain only baryonic matter and have roughly constant M/L, a flatter relation, $L \propto \sigma^{2.7}$, is expected (Dekel & Silk 1986).

Clusters of galaxies are ideal for studying scaling relations as they provide a large number of galaxies of different types, at a common distance, different environments within the cluster, and allow one to assess the interaction with the intracluster medium (ICM). Since the Coma cluster is one of the nearest, rich and dense clusters, it has been a popular target for studies of scaling relations among galaxies including the FJ relation (Jørgensen, Franx & Kjaergaard 1996; Moore et al. 2002, hereafter MLKC02; Graham & Guzmán 2003).

The FJ relation for faint ellipticals in the Coma cluster has been studied by Matković & Guzmán (2005, hereafter MG05) and Cody et al. (2009, hereafter Co09), using Wisconsin Indiana Yale NOAO (WIYN)/HYDRA (multifibre) spectroscopy. Both MG05 and Co09 find $L_R \propto \sigma^{2.0\pm0.3}$ for dwarf ellipticals even though these studies have only 10 galaxies in common whose σ measurements differ by up to $\sim$30 per cent for the faintest galaxies. Thus, it is important to obtain high signal-to-noise ratio (S/N) data to measure velocity dispersions for dwarf galaxies at fainter magnitudes.

In this paper, we use the high spectral resolution of the DEep Imaging Multi-Object Spectrograph (DEIMOS) (Faber et al. 2003) on the Keck II telescope to measure the velocity dispersions for a sample of 41 faint elliptical galaxies in the core of the Coma cluster. Of these galaxies, 15 are common with the samples of MG05, Co09 or both, and for the remaining 26, these are the first velocity dispersion measurements. The current DEIMOS measurements extend the study to luminosities in the range $-16.5 < M_R < -15$, about 1 mag fainter than the limit reached by the WIYN/HYDRA data in previous studies of Coma dwarf galaxies.

This paper covers mainly the observations and the technical part of the analysis. The emphasis is on the reliable estimate of the uncertainties in measuring the internal velocity dispersion of galaxies. In Section 2 we describe the observations, the spectroscopic setup and the data reduction. Section 3 is dedicated to the measurement of radial velocities and the velocity dispersions. The error analysis is described in Section 4. The results of the analysis and the FJ relation are presented and discussed in Section 5.

Throughout this paper, the distance modulus of the Coma cluster is considered to be 35.00 mag (Carter et al. 2008).

2 OBSERVATIONS

2.1 Source selection

Galaxies were selected using the photometry from Adami et al. (2006). The ($B - R$) versus R colour–magnitude relation was constructed, and the red sequence identified and fitted by a linear rela-

tion. Galaxies were then selected from within a region $\pm 3\sigma$ from this relation, with a magnitude range $-19 < M_R < -16$, or $16 < R < 19$. Images from the *Hubble Space Telescope* (*HST*)/ACS Coma Treasury Survey (Carter et al. 2008) were then used to reject a very small number of galaxies with obvious spiral structure. However, not all candidates fell within the footprint of the completed survey (which was truncated owing to ACS failure) so some late-type galaxies may remain in the sample. The masks were then designed at the University of Hawaii as a compromise between two programmes: the velocity dispersions programme described here, and a separate programme to measure redshifts of a sample of low surface brightness galaxies. The requirement that the spectra from different slits should not overlap, and the need for sufficient slit length to enable sky subtraction, places considerable restriction on the number of galaxies one can observe in each mask.

2.2 Spectroscopic setup

The observations were carried out on the night of 2007 March 19, using DEIMOS on the Keck II telescope. The outer dimensions of the rectangular DEIMOS field are 16.7×5.0 arcmin^2 and all observed spectra are mapped on to a 2×4 mosaic of 2K $\times$ 4K CCDs (two CCDs for each spectrum). We used a 1200 G grating (1200 grooves mm^{-1} BK7, gold coated and blazed at 7760 Å). The nominal central wavelength at the centre of the mask was 8700 Å, although of course the central wavelength of a given spectrum depends upon the position of that slitlet in the mask. Although slitlets for the redshift survey observations were drilled at a variety of widths, all of those for the velocity dispersion project described here had widths of 0.7 arcsec. Reciprocal dispersion is 0.33 Å pixel^{-1}, giving a spectral resolution [full width at half-maximum (FWHM)] of 1.6 Å and a resolving power $R \sim 5000$. This equates to an instrumental velocity width of $\sim$25 km s^{-1}, allowing us to measure velocity dispersions down to $\sim$15 km s^{-1} in spectra with S/N $\geq$15 pixel^{-1}. The velocity dispersions of galaxies in the $17 \leq R \leq 19$ dE sample are expected to range between 10 and 80 km s^{-1}. The spectral range covered is approximately 7500–10 000 Å, although it depends upon the slit position in the mask. This wavelength range is dominated by the very deep calcium II triplet (CaT) absorption lines at 8498.02, 8542.09 and 8662.14 Å, which depend only weakly upon metallicity and therefore provide an ideal range over which to measure the kinematic properties of low-luminosity galaxies. A GG495 filter was used to block out the contamination from the second-order blue spectrum.

Two masks were observed for each of two pointings, and the exposure time for each mask was in the range 6030–6600 s. A summary of these observations is presented in Table 1. In addition, a number of potential template stars, and flux calibration stars, were observed using a 0.7 arcsec width long slit during twilight at the beginning and end of the night. Wavelength calibration arcs and observations of internal flat-fielding lamps were also made at the beginning of the night.

We observed 11 standard stellar spectra of which only two templates were reliable for measurements in this study. The other stellar templates were excluded because they either were not G/K-type stars or were affected by noise near the Ca triplet lines.

2.3 Data reduction

The spectra of dwarf galaxies and template stars were reduced using the IDL spec2d pipeline developed by the DEEP2 Galaxy Redshift Survey team at the University of California–Berkeley for

Table 1. List of the exposures on the galaxy masks. In column 5, we give the number of slits drilled at 0.7 arcsec width, specifically for the velocity dispersion programme, excluding those drilled at larger widths for redshift measurements of low surface brightness galaxies. In column 6, we give the total number of slits per mask.

| Mask | Mask centre (J2000) | | Exposure | No. of slits | |
| | RA | Dec. | time (s) | dEs | Total |
(1)	(2)	(3)	(4)	(5)	(6)
Coma1-1	12:59:57.83	27:59:30.6	6600	24	105
Coma1-2	12:59:57.83	27:59:31.2	6600	15	109
Coma2-1	13:00:04.04	27:54:52.2	6600	22	101
Coma2-2	13:00:04.04	27:54:52.2	6030	14	103

that project [see Davis et al. (2003) for more information]. The pipeline performs the flat-fielding using internal quartz flats and the wavelength calibration using the ArKrNeXe arc lamps. The sky subtraction and the data extraction to 1D spectra are also done within the pipeline. For our purpose here, all spectra are not flux calibrated and all partially remaining sky emission lines, particularly near the Ca triplet lines, were manually removed. In this manual process, for each galaxy spectrum, we checked the wavelength of the remaining bright emission lines with the catalogues of the sky emission lines and then we replaced the verified sky emission lines with the continuum fitted underneath the spectrum. Each spectrum was originally located on two CCDs. In order to join the blue and red parts of each 1D spectrum, the average value of the nearest 50 pixels to the CCD gap was calculated and the offset was used to construct the conjoined thorough 1D spectrum. An example of final 1D spectra from DEIMOS in the range ~8300–9000 Å is shown in Fig. 1. In this paper all spectral S/N values are estimated per pixel (i.e. 0.33 Å).

3 THE MEASUREMENT OF RADIAL VELOCITY AND VELOCITY DISPERSION

There are 49 galaxies in our DEIMOS sample with spectroscopically confirmed Coma membership (Marzke et al., in preparation). The CaT absorption lines for eight galaxies either were coincident with gaps in the CCD mosaic or had too low S/N to make reliable measurements and therefore were taken out of the sample. We thus used 41 spectra with identified CaT lines with S/N ranging from 5 to 87. Fig. 1 shows four of the sample spectra.

The line-of-sight radial velocities and velocity dispersions, σ, were measured using the PPXF[1] software developed by Cappellari & Emsellem (2004). The PPXF technique works in pixel space and uses Gauss–Hermite series to extract the radial velocity and velocity dispersion simultaneously by minimizing the χ^2 which is defined as

$$\chi^2 = \sum_{n=1}^{N} \frac{G_{\mathrm{mod}}(x_n) - G(x_n)}{\Delta G(x_n)}, \qquad (1)$$

where $G(x_n)$ and $G_{\mathrm{mod}}(x_n)$ are the original and the modelled galaxy spectra, respectively. $\Delta G(x_n)$ is the error in the observed galaxy spectrum and N is the number of good pixels used in the fitting process.

First, both galaxy and stellar template spectra are rebinned in wavelength space [$x = \ln(\lambda)$]. A range of model spectra are obtained by convolving the stellar template with a broadening func-

---

[1] Penalized pixel fitting.

tion, which takes into account the true galaxy radial velocity and a range of trial velocity dispersions. The minimization is then carried out over this range of broadened templates. Compared to the other methods, Cappellari & Emsellem showed that for a low S/N, the use of maximum penalized likelihood suppresses the noise effect in the solution. This makes the PPXF method robust for objects with low S/N such as our dwarf galaxies.

PPXF enables us to use any desired wavelength range for measurements (see Fig. 2 for example). In order to benefit from the high S/N part of the spectrum, we chose the rest-frame spectral range of 8450–8700 Å which covers the CaT features. All galaxy spectra and stellar templates are continuum subtracted. Due to the noise, for a few faint galaxies ($M_R > -16$ and S/N < 15), the measured velocity dispersion is very sensitive to the selected wavelength range and therefore high errors are expected in the final results.

In order to provide realistic initial values of radial velocity to PPXF, the IRAF FXCOR package was used to obtain the relative velocity for each selected pair of the galaxy and template spectra. FXCOR is based on the Fourier cross-correlation technique developed by Tonry & Davis (1979). The location of the highest peak of the correlation function represents the most probable blueshift/redshift value of the galaxy. Although the FXCOR task can measure velocity dispersions, it also requires simulations of multiple spectra in order to construct a proper relation between the width of the highest peak of the correlation function and the real velocity dispersion of the galaxy. Such simulations are not necessary when using PPXF. Other advantages of the PPXF package include the use of multiple stellar templates, where these are optimized and weighted, and shorter computing time.

Of the 11 stellar templates observed by DEIMOS, only two spectra (i.e. HD 44007 and HD 45282) had a high enough S/N near the strong CaT absorption lines to be used in our analysis. Therefore, we added more G/K-type spectra from the Indo-US Coudé Feed spectral library (Valdes et al. 2004). For practical reasons, especially computing time, we used 11 stellar templates (see Table 2) to perform single template analysis and simulations. To find the best optimal synthetic template, a set of 80 mixed templates were used to finalize the results.

The first PPXF run shows a significant difference in the velocity dispersion values when different templates in Table 2 are used. The scatter in σ values gives an estimate of the uncertainty due to the multistellarity of galaxies. To reduce the effect of stellar population on the measured σ, a set of 50 mixed stellar templates (hereafter Set50) from the Indo-US library consisting of G/K stars were simultaneously given to PPXF and the best combination was obtained by optimizing the χ^2 values. For each galaxy spectrum, the Set50 PPXF run significantly improves upon a single template, and the χ^2 values are improved by 10 per cent (on average), compared with 7 per cent intrinsic statistical χ^2 deviation of a single template PPXF run. This also points at the multistellar nature of galaxy spectra. The impact of the stellar template mismatch is discussed in Section 4.2. In 44 per cent (20 per cent) of the cases, the χ^2 is improved by more than 10 per cent (20 per cent).

To explore the sensitivity of the final results to the number of templates, a set of 80 templates (hereafter Set80), consisting of Set50 and 30 more G/K-type templates, also chosen from the Indo-US library, were used. Comparing the resulting velocity dispersion for Set50 and Set80 indicates that for 36 of 41 galaxies, the discrepancy in the results is less than 2 per cent and it does not exceed 10 per cent for the rest. Although a larger number of templates improves the results, it dramatically increases the computation time. Moreover, the use of Set80 instead of Set50 does not improve the χ^2
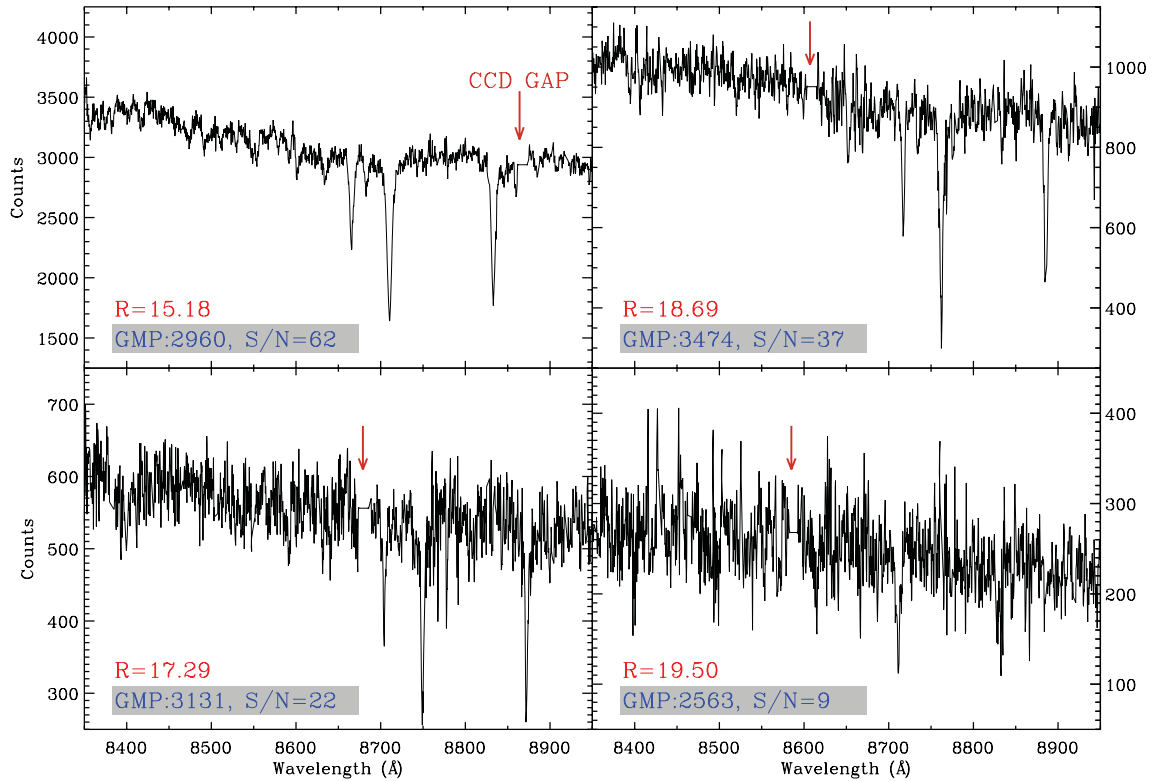
Figure 1. Example of galaxy spectra in the sample with different values of S/N. All S/N values are estimated per pixel. The Godwin, Metcalfe & Peach (1983; GMP) ID and *R* magnitude are given for each galaxy. In each panel, the arrow shows the location of the CCD gap in the spectrum.
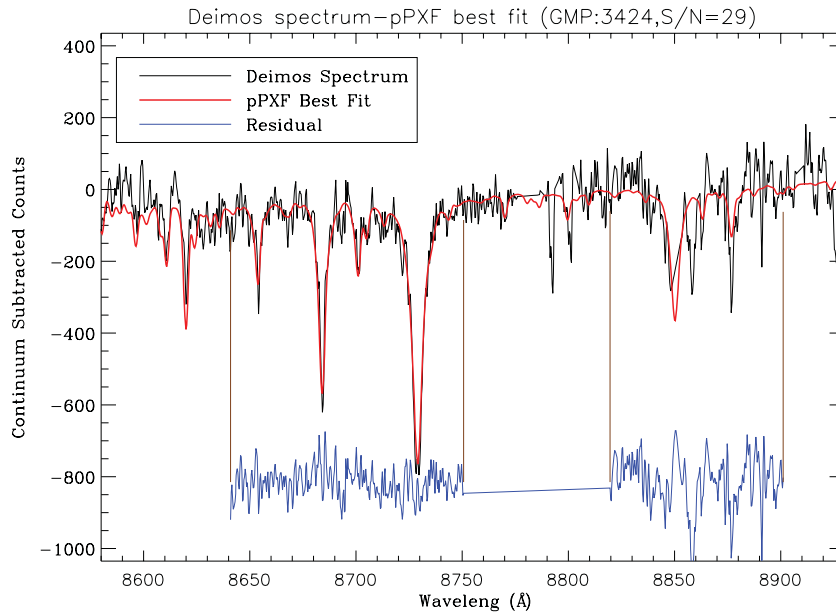

Figure 2. An example of PPXF fit to a galaxy (GMP 3424) from the 2007 DEIMOS run. Thin black is the observed spectrum, and the thick black (red) line is the best PPXF fit using a single stellar template. The residuals over the fitted region are also shown (blue). The S/N for this spectrum is 29, and we find $V_r = 5596 \pm 7\,\mathrm{km\,s^{-1}}$ and $\sigma = 27 \pm 9\,\mathrm{km\,s^{-1}}$.

significantly (i.e. ∼1 per cent on average), and thus we did not continue adding more templates to Set80. We find that all galaxies are modelled with a combination of at least two templates. For 80 per cent of the galaxies in our sample, more than two templates describe the spectra, and in 30 per cent of the cases, a mixture of more than four templates were chosen. The results of the Set80 PPXF run are

assigned to each galaxy and used for the rest of this paper (see Table 6).

When we used Set80 (Set50), 38 (14) templates are not chosen to describe any of sample galaxies. Six of 26 used templates from Set50 are not chosen again by PPXF when using Set80. Of 30 added templates to Set50, only 14 contribute to describe at least one

Table 2. The list of stellar templates, their spectral type and their stellar parameters (i.e. effective temperature, metallicity and surface gravity). $T_{\rm eff}$ and g are in terms of K and cm s^{-2}. All stellar parameters are taken from the Indo-US library. These templates were used to perform the initial measurements and simulations.

Library	ID [HD]	Spectral type	$T_{\rm eff}$	[Fe/H]	log (g)
DEIMOS	44007	G5IV	4850	−1.71	2.00
(this study)	45282	G0V	5280	−1.52	3.12
Indo-US	44007	G5IV	4850	−1.71	2.00
	45282	G0V	5280	−1.52	3.12
	117876	G8III	4582	−0.50	2.25
	161797	G5IV	5411	0.16	3.87
	223-65	G2IV	5350	−0.59	3.50
	142198	K0III	4700	−0.08	2.99
	48433	K1III	4425	−0.24	1.35
	6497	K2III	4421	0.02	2.80
	78479	K3III	4509	0.57	2.54

Table 3. The list of most frequent stellar templates used in the analysis with Set50 and Set80. These templates are used to reproduce more than two galaxy spectra. Columns 3, 4 and 5 show the effective temperature, metallicity and surface gravity of each star, respectively. Stellar parameters are taken from the Indo-US library. The list is sorted in terms of the metallicity. Columns 6 and 7 indicate the utilization frequency of the templates of Set50 and Set80, respectively.

ID (HD)	Spectral type	$T_{\rm eff}$ (K)	[Fe/H]	log (g) (cm s^{-2})	Set50 (per cent)	Set80 (per cent)
63791	G0I	4700	−1.81	1.70	17	10
44007	G5IV	4850	−1.71	2.00	5	7
187111	G8IV	4429	−1.54	1.15	24	22
45282	G0V	5280	−1.52	3.12	24	29
81192	G8III	4582	−0.70	2.75	7	2
210752	G0V	5910	−0.64	4.25	12	20
G_241-18	G5V	5511	−0.61	4.00	–	10
G_165-11	G0V	5725	−0.56	4.00	20	17
201099	G0V	5872	−0.50	4.06	–	7
157214	G0V	5676	−0.41	4.33	–	7
99167	K5III	3930	−0.38	1.61	10	10
82210	G5III	5250	−0.34	3.42	7	5
83787	K5III	4000	−0.18	1.60	17	22
169414	K2III	4450	−0.16	2.67	7	7
186486	G8III	4980	−0.11	3.08	12	15
225212	–	3700	−0.03	0.80	10	2
150680	G0IV	5825	0.00	3.80	–	7
237903	–	4070	0.00	4.70	46	20
17925	K2V	5091	0.10	4.60	10	7
161797	G5IV	5411	0.16	3.87	10	10
63302	K3I	4500	0.17	0.20	–	10
182293	K3IV	4486	0.25	3.00	20	17
G_196-9	K5V	4000	0.28	4.50	–	24
130705	K4III	4350	0.51	2.10	22	20

galaxy spectrum in the Set80 PPXF run. In Table 3, a list of stellar templates which are used to reproduce more than two galaxy spectra is provided.

4 ERRORS AND UNCERTAINTIES

In this section we discuss the accuracy of our measurements and the sources of uncertainties.

4.1 Statistical uncertainties

One important source of uncertainty is the statistical error which is highly correlated with the S/N. We adopt a 'bootstrapping' technique to quantify this uncertainty. We simulate an ensemble of galaxy spectra covering the observed range of S/N, the broadening parameter (σ) and the velocity shift (V_r), using the stellar template spectra. To achieve a desired σ, the stellar template spectrum is convolved with a Gaussian function. Then random noise is added to achieve the desired S/N. For each observed galaxy spectrum, a set of 300 realizations were generated, noting that increasing the number of realizations does not alter the results. We then apply the same measurement technique.

The measurements on each simulated set are carried out with the same initial parameters as used in the measurement of the original spectrum. Although the input spectral broadening, $\sigma_{\rm in}$, for each set of simulated spectra is the same, the measured value ($\sigma_{\rm m}$) can be different, due to the noise, and forms a Gaussian distribution around a mean value. The mean of the measured values is not necessarily the same as the input $\sigma_{\rm in}$ value, due to a systematic shift. In general, for all templates in Table 2 and all probable S/N values, we obtained $P(\sigma_{\rm m}|\sigma_{\rm in})$ (i.e. the probability of obtaining $\sigma_{\rm m}$ for the simulated galaxy with the initial velocity dispersion of $\sigma_{\rm in}$). To perform the simulations, for any given S/N, $\sigma_{\rm in}$ is chosen to have a range of discrete values 10–100 km s^{-1}. For other values of $\sigma_{\rm in}$, we used the polynomial functions to obtain the mean and rms of the measured velocity dispersion. This is explained in detail in section 3.3 of Co09. Fig. 3 shows the relation between the input velocity dispersion and the rms of the measured σ for different S/N values. As expected, $\sigma_{\rm m}$ is more uncertain when the S/N decreases or velocity dispersion increases. The left-hand panel of Fig. 3 indicates that the uncertainty in σ is higher when the template for the velocity dispersion measurement is from a different instrument than that from which we simulated the galaxy spectra.

In reality, we have only one spectrum of each galaxy based on which we estimate its velocity dispersion, $\sigma_{\rm m}$. Similarly, we can assume that of each set of simulated spectra with given S/N ratio and $\sigma_{\rm in}$, we only have access to one spectrum and its measured velocity dispersion, $\sigma_{\rm m}$. Therefore, to derive the initial velocity dispersion ($\sigma_{\rm in}$) and its uncertainty, we have to invert the above statistics and find $P(\sigma_{\rm in}|\sigma_{\rm m})$. This is what needs to be done for any given original galaxy spectrum. Having all $P(\sigma_{\rm m}|\sigma_{{\rm in},i})$ for each $\sigma_{{\rm in},i} \in \{1, 2, 3, \ldots, 200\,{\rm km\,s}^{-1}\}$, the probability of finding the true velocity dispersion, $\sigma_{\rm true}$, for any measured velocity dispersion, $\sigma_{\rm m}$, is given by (Co09)

$$P(\sigma_{{\rm true},k}|\sigma_{\rm m}) = P(\sigma_{\rm m}|\sigma_{{\rm in},k}) \Big/ \sum_{i=1}^{200} P(\sigma_{\rm m}|\sigma_{{\rm in},i}), \tag{2}$$

where $\sigma_{{\rm in},i} = \sigma_{{\rm true},i} = i\,{\rm km\,s}^{-1}$. Fig. 4 shows four examples of the probability density of true velocity dispersion for any given measured value, $\sigma_{\rm m}$. In order to illustrate the dependence of the results upon the selected templates, for panels (a) and (b) of Fig. 4 we used the stellar template HD 161797 (G star), and for panels (c) and (d) we used HD 78479 (K star). As seen, the peak centre of the probability distributions is not centred upon the true velocity dispersion. This systematic shift is mainly due to the template mismatch and other systematics caused by using different instruments for simulation and measurement. As shown in Fig. 4, the location of the peak centres changes when we use different templates for measurements, and for a given template it is independent of S/N. For any given velocity dispersion and stellar template, the S/N value
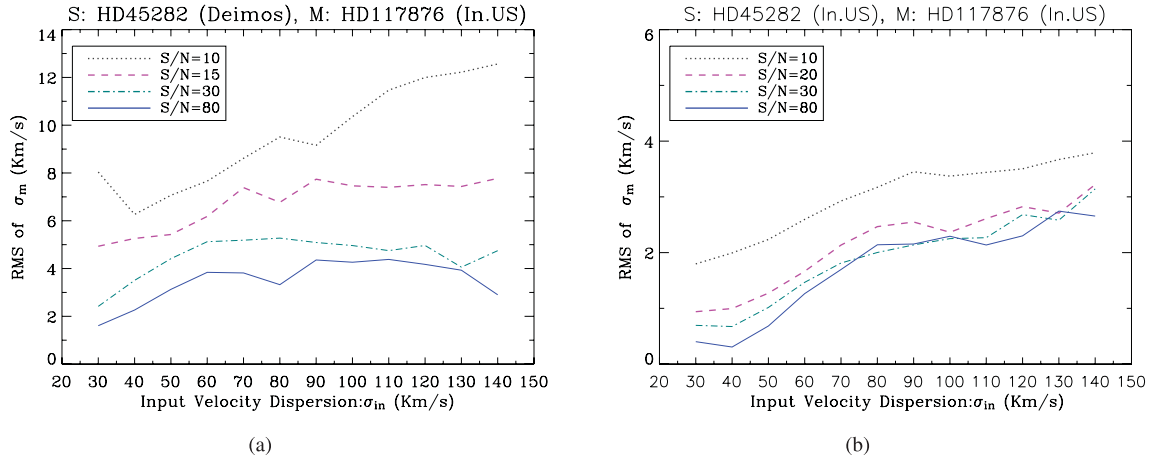
Figure 3. The rms of measured velocity dispersion is plotted against the input velocity dispersion (σ_{in}) used to run simulations. 300 simulated galaxies are generated for each S/N and σ_{in}. In both plots, the templates are the same. In plot (a), DEIMOS and Indo-US spectra were used as simulation and measurement templates, respectively. As one expects, lower S/N and greater σ_{in} result in bigger inaccuracies. In plot (b), both templates were selected from the Indo-US library. Comparing the two plots, it is clear that when using different instruments for the simulation and measurement, the typical value of the uncertainties is greater.
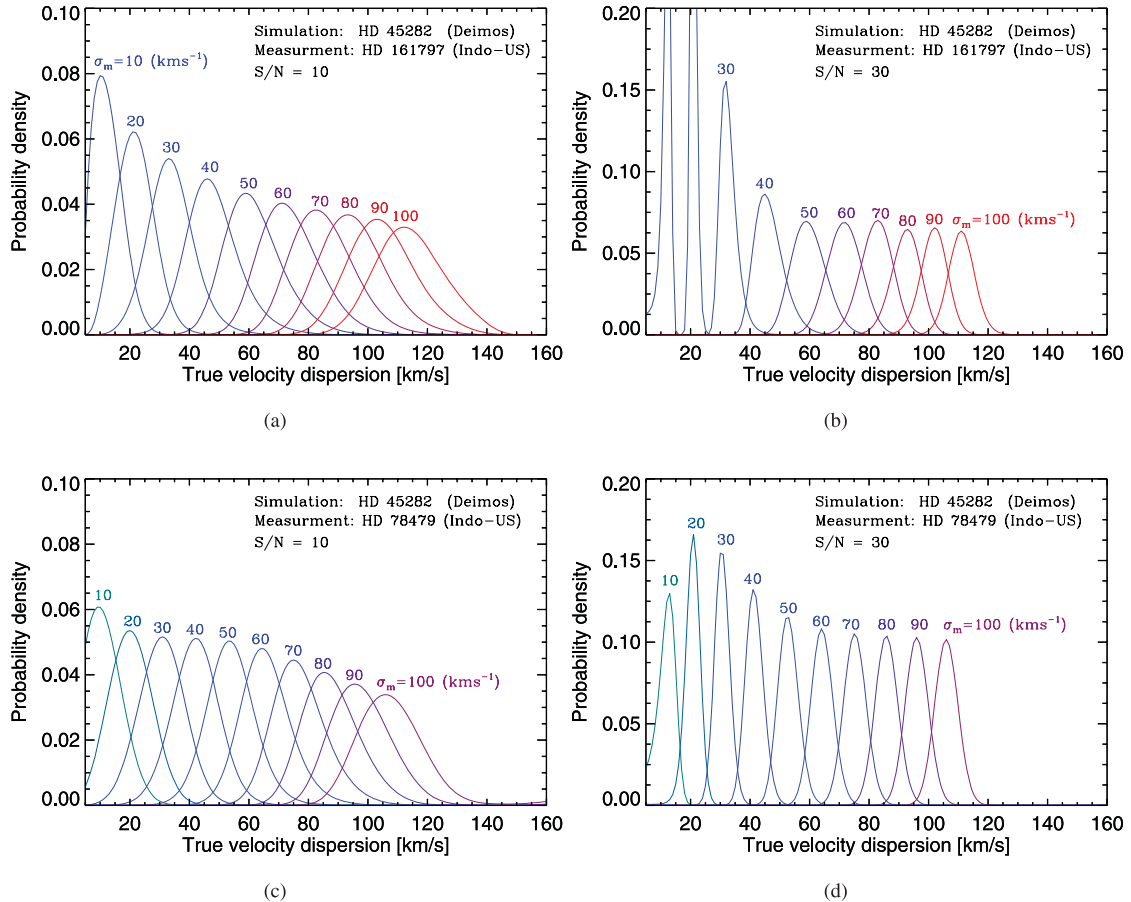

Figure 4. The distribution of true velocity dispersion for measured dispersion, σ_m. Different instruments and templates are chosen to consider all sources of uncertainty. For each $\sigma_{in} = 10, 20, \ldots, 100 \, \mathrm{km\,s^{-1}}$, 300 simulated spectra are generated using HD 45282. In each diagram, the S/N of the simulated spectra is constant. The S/N in left- and right-hand panels are 10 and 30, respectively. To see the dependence of the uncertainties upon the stellar template used for measurements, measurements are carried out with HD 161797 (G star) and HD 78479 (K star) in the top and bottom panels, respectively, and then the statistics are inverted to find $P(\sigma_{true}|\sigma_m)$. The width of the Gaussian peaks corresponds to the statistical uncertainties (see Section 4.1) and the systematic shift of the peaks along the axis of true velocity dispersion is due to the fact that we used different templates and different instruments for simulation and measurement (see Section 4.2 for more detailed analysis). We see higher uncertainties for larger σ_m values. To estimate the final uncertainty of the measured dispersions, the 1σ width of each corresponding peak and its systematic shift are added in quadrature.

affects mainly the statistical uncertainty and therefore the width of the Gaussian peaks.

To estimate the statistical inaccuracy of the final results, 1σ uncertainty is derived for each peak of the probability density. The simulated galaxy sample is generated based on the same templates used for the measurements. We performed the above procedure for all individual stellar templates in Table 2 which are initially used to measure σ and V_r of the sample galaxies. Since all sample galaxies are observed with DEIMOS, in another run of simulations we applied DEIMOS stellar templates (i.e. HD 44007 or HD 45282) for simulation and Indo-US templates for measurement. This method makes our analysis more realistic and enables us to study any additional sources of error due to the instrumental differences. When we apply individual stellar templates, the change in measured velocity dispersions for each galaxy is larger than the corresponding statistical error and we attribute this to the effect of the template mismatch which is investigated in Section 4.2.

4.2 Template mismatch and other sources of uncertainties

The velocity dispersion measurement is highly sensitive to the width of the spectral lines in the stellar template based on which the measurements are carried out. The width of the lines is determined by chemical compositions, temperature and the age of the stars (Lejeune, Cuisinier & Buser 1997; Schulz et al. 2002, and references therein). On the other hand, any galaxy is a composite of different stellar populations and thus lack of any prior knowledge about the exact dominant stellar type is an additional source of uncertainty.

Velocity dispersion measurements of galaxies using the red part of the spectrum are reported to be less sensitive to systematic errors compared with measurements using the blue and visual spectral regions (Pritchet 1978). Our measurements are based on CaT lines which depend weakly on metallicity in metal-rich stars (Mallik 1994). However, for metal-poor stars, the effect of the metallicity on CaT lines could not be neglected (Díaz, Terlevich & Terlevich 1989; Smith & Drake 1990; Zhou 1991; Jørgensen, Carlsson & Johnson 1992; Starkenburg et al. 2010) and therefore CaT lines are also employed as a metallicity indicator (Carrera et al. 2007; Michielsen et al. 2007; Foster et al. 2010). Moreover, evidence has been found for significant anticorrelation between CaT indices and central velocity dispersion of elliptical galaxies (Cenarro et al. 2003). Therefore, template mismatch may have a significant impact on the final results of σ measurements, and although our measurements are based on 80 G/K-type stellar templates, we still need to quantify the uncertainty due to the template mismatch.

Another source of uncertainty appears when the galaxy and template spectra are observed with different instruments. This error is due to the difference in the sensitivity and resolution of the instruments. The FWHM spectral resolution of the Indo-US templates is 1.0 Å and that of DEIMOS is about 1.6 Å for the wavelength range in this study. To take this into account, a proper Gaussian function is convolved with the higher resolution spectrum corresponding to the difference in the spectral resolution. In addition, the sampling rates of Indo-US and DEIMOS spectra are 0.4 and 0.3 Å pixel^{-1}, respectively. Although PPXF resamples and rebins both template and target galaxy spectra to account for this difference, this still may lead to systematic errors in the final results.

Due to the limited number of stellar templates observed with DEIMOS, we are unable to disentangle the uncertainty due to instrumental differences from the uncertainty due to template mismatch. As shown in Fig. 4, the cumulative effect of both template mismatch and difference in the instruments (Indo-US and DEIMOS charac-

teristics) causes systematics in the measured values. Therefore, the shifts seen between the σ_{in} and σ_m are due to both effects. Similar diagrams are generated for any selected Indo-US and DEIMOS stellar templates. All pairs of different templates and instruments are considered to study all sources of error and their contributions.

We generated a comprehensive set of simulated data using all stellar templates in Table 2 according to the method explained in Section 4.1. In this method, measurements and simulations are carried out with different templates of the same instrument or with similar templates from different instruments. The resulting velocity dispersions and given initial values are then compared after performing the cross-measurements on the simulated data with various noise levels. Two examples are presented in Fig. 5 which show the deviation of the measured values, σ_m, from the true input values, σ_{in}, for a given velocity dispersion. All simulations are carried out without adding any noise in order to explore the template mismatch effect. We obtained higher systematic errors by choosing the templates from different instruments. All curves in the left-hand panel of Fig. 5 illustrate this fact except for two curves A and B for which DEIMOS templates were used for measurements.

As expected, no significant systematic shift arises when the same template from the same instrument is used for simulation and also the measurement. Typically, the relative systematic errors tend to be constant and to slightly increase, respectively, for higher and lower velocity dispersions. To study the sensitivity of the systematics to the S/N, all aforementioned simulations were repeated with random noise added. The left- and right-hand panels of Fig. 6 show the results for the same curves in the corresponding panels of Fig. 5 including different noise levels. As seen, except for a very low S/N (i.e. S/N $\lesssim$ 10 per pixel), the systematic errors are not affected by the value of S/N. We repeated the procedure several times for different wavelength ranges and any pair of templates and instruments in Table 2. In all cases, for $\sigma > 20\,\mathrm{km\,s^{-1}}$, the effective mean value of all uncertainties does not exceed 20 per cent of the true value of the velocity dispersion.

Two examples are presented in Tables 4 and 5. In Table 5, we noted higher measured σ values for HD 44007 and HD 45282 compared to the measured values using the other templates, even though HD 44007 and HD 161797 (i.e. the template used for simulation) have the same spectral type. We attribute this to lower metallicity (i.e. [Fe/H]) of both HD 44007 and HD 45282 compared to the other templates (see Table 2) and consequent systematic errors. As shown in the second and third columns of Table 5 (low metallicity stars with [Fe/H] < -1.5), for $\sigma_{in} > 20\,\mathrm{km\,s^{-1}}$, the average relative discrepancy between the measured values, σ_m, and input values, σ_{in}, is 20 per cent. This value is reduced to 10 per cent for the other templates. Further evidence for systematic uncertainties in the presence of metallicity differences is seen when measuring the velocity dispersion of our sample galaxies with HD 44007 and HD 45282 in a single template run which results in 25 per cent larger values, on average, compared to those measured using multiple templates. This discrepancy is reduced to ~5 per cent, on average, for single PPXF run with the other seven templates of Table 2.

In order to examine the effect of the galaxy and stellar template metallicity on measured velocity dispersions, we used 21 stellar templates with the same spectral type (i.e. G8III) from the Indo–US library and different metallicity. As shown in Fig. 7, we used the stellar spectra HD 45282, observed by DEIMOS, to simulate galaxies with desired velocity dispersions, i.e. $\sigma_{in} = 10, 30, 50, 80$ and $100\,\mathrm{km\,s^{-1}}$. In each case, 300 simulated spectra with S/N = 30 were created. Then, the velocity dispersions of the simulated galaxies were measured using the stellar templates
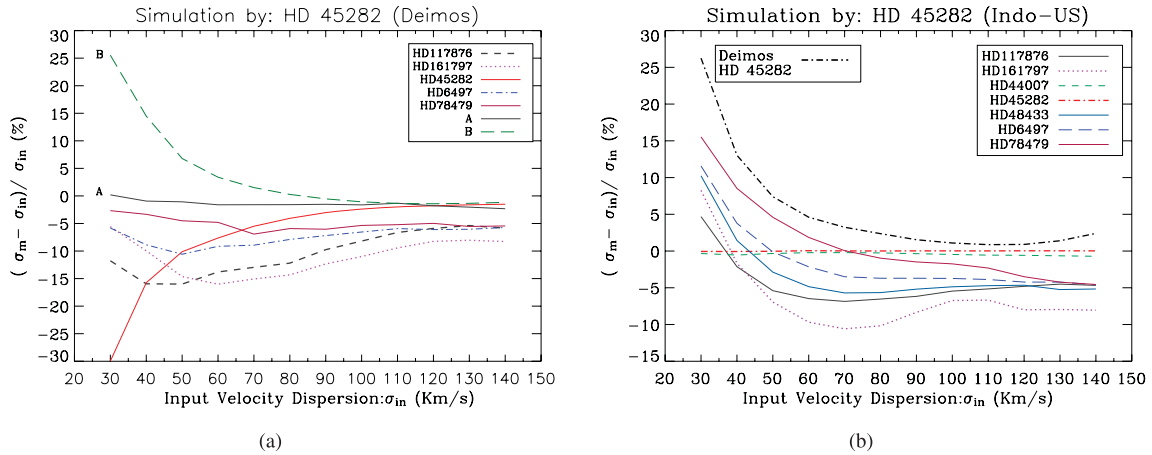
Figure 5. The relative difference between the measured velocity dispersion and the given input value is plotted for different templates. In panel (a), the DEIMOS spectrum HD 45282 is used for simulation and measurements are carried out with Indo-US and DEIMOS spectra. The template spectrum is broadened with the desired broadening factor (σ_{in}) and no noise is added in this stage to see only the effect of template mismatch. Curve A shows the results of the same template used for simulation and measurement (i.e. DEIMOS HD 45282), and as seen, the discrepancies are negligible. The measurements using another DEIMOS template (i.e. HD 44007) lead us to curve B with larger discrepancies for low dispersions. Other curves show the measurement results using Indo-US templates. Panel (b) is the same as panel (a) except for the instrument used for simulation. As expected, there is no discrepancy when the same template is used for measurement (i.e. Indo-US HD 45282). The black dash–dotted line in the right-hand panel shows the results of measurements with the DEIMOS template (HD 45282). As a result, the effect of mismatch and other uncertainties is less than 15 per cent for $\sigma_{in} > 40 \, \mathrm{km \, s^{-1}}$. Ignoring both templates HD 44007 and HD 45282 whose results behave differently regardless of the selected instrument, the average mismatch error is about 7 per cent. We noted that the metallicity of these two templates is significantly less than the other templates (see Table 2).
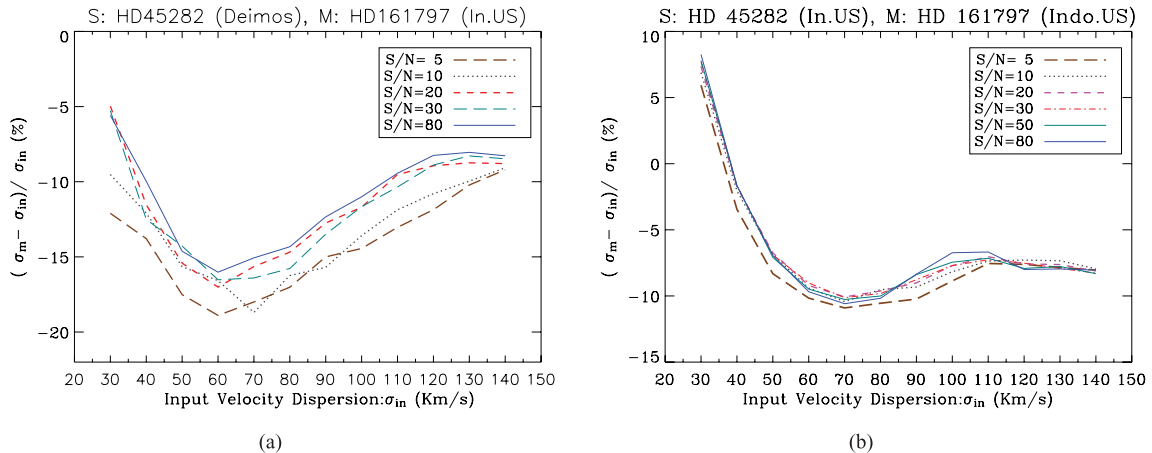

Figure 6. Same as Fig. 5 except that we used only one of the stellar spectra for velocity dispersion measurements and the S/N of the simulated spectra vary. The relative differences of measured and input velocity dispersions are plotted for different S/N values. This shows that for S/N > 10 per pixel, mismatch and other uncertainties are not affected by the signal level, which means that the effect of S/N enters only through the statistical uncertainties. 300 simulated spectra were generated for each pair of S/N and σ_{in}. The simulations for left- and right-hand panels were carried out with DEIMOS and Indo-US spectra of HD 45282. The same template (HD 161797) was used for measurements in both panels.

with the same spectral type but different metallicities. Fig. 7 shows that differences between the measured and input velocity dispersion are independent of the template metallicity within ~2 km s⁻¹ uncertainty in measured velocity dispersions. Due to the template mismatch effect, in each panel of Fig. 7, there is an offset between the given velocity dispersion and the mean value of the measured velocity dispersions using the templates with different metallicities. This offset is due to the template mismatch effect, and for a given spectral type, it seems to be independent of the template metallicity.

As shown in Fig. 8, we used the mixed stellar templates, i.e. Set80, for measuring the velocity dispersion of simulated galaxies with

different metallicities. To perform the simulations, we broadened the stellar templates with different metallicities (i.e. the G8III-type stars used in Fig. 7) according to desired input velocity dispersions. At very low velocity dispersion (i.e. $\sigma_{in} = 10 \, \mathrm{km \, s^{-1}}$), the mean value of the measured velocity dispersion for all simulated spectra with different metallicities is 11.5 km s⁻¹. For $\sigma > 10 \, \mathrm{km \, s^{-1}}$, the measurements result in the same value as the input values and are independent of metallicity. As a conclusion, based on the simulations, using the mixed stellar templates results in more reliable measurements and reduces the effect of template mismatch. To confirm these results, we measured the velocity dispersion of the simulated

Table 4. The measured velocity dispersion using different stellar templates with different spectral types (see the first row). The first column represents the input velocity dispersion based on which the simulation is carried out. Under each template, the measured values are reported in terms of km s^{-1}. The DEIMOS star spectrum HD 44007 is used to generate the simulated galaxy spectra and all measuring templates are picked up from the Indo–US library. For each set, the average of the results is calculated and no noise is added to only estimate the effect of template mismatch which is the offset between the initial and measured values. In the last column, for each row the maximum discrepancy [i.e. $\Delta_{max} = |\sigma_m - \sigma_{in}|/\sigma_{in}$ (per cent)] is calculated for $\sigma_{in} > 10$ (km s^{-1}), in which σ_{in} is the initial velocity dispersion used for the simulation and σ_m is the measured value. For $\sigma_{in} > 20$ (km s^{-1}), the average discrepancy is about 7 per cent and for $\sigma_{in} > 100$ (km s^{-1}) it is almost 3 per cent.

σ_{in} (km s^{-1})	HD 44007 (G5IV)	HD 45282 (G0V)	HD 117876 (G8III)	HD 161797 (G5IV)	HD 223-65 (G2IV)	HD 142198 (K0III)	HD 48433 (K1III)	HD 6497 (K2III)	HD 78479 (K3III)	Δ_{max} (per cent)
10	1	11	5	17	14	8	14	12	5	–
20	11	14	20	22	17	20	22	21	22	45
30	26	25	27	29	30	27	28	28	29	17
40	35	36	34	35	40	34	35	36	39	15
50	46	47	43	43	42	43	44	45	49	16
60	57	57	52	51	52	53	53	55	58	15
70	68	68	62	60	62	62	63	64	67	14
80	79	79	72	69	72	72	80	74	76	14
90	89	90	82	79	83	83	83	84	86	12
100	100	101	93	89	93	100	93	94	100	11
110	111	112	104	100	110	104	110	105	110	9
120	122	123	120	110	114	115	114	120	116	8
130	133	134	125	120	125	126	130	125	126	8
140	144	146	136	130	140	136	134	140	136	7

Table 5. Same as Table 4. The template HD 161797 is used for simulation and all templates are selected from the Indo-US library. Looking at column 5, as one expects, no discrepancy between the initial and measured value is found. The two last columns (Δ_a and Δ_b) show the maximum discrepancies as in Table 4. Column Δ_a is calculated for all applied templates and since the templates HD 44007 and HD 45 282 result in large discrepancies, the column Δ_b is created ignoring them. Considering all templates, for $\sigma_{in} > 20$ (km s^{-1}), the average discrepancy is about 10 per cent and for $\sigma_{in} > 100$ (km s^{-1}) it is almost 7 per cent. The metallicities of HD 44 007 and HD 45 282 are lower than those of the other templates and therefore result in measuring larger σ_m compared to the other templates (see Table 2).

σ_{in} (km s^{-1})	HD 44007 (G5IV)	HD 45282 (G0V)	HD 117876 (G8III)	HD 161797 (G5IV)	HD 223-65 (G2IV)	HD 142198 (K0III)	HD 48433 (K1III)	HD 6497 (K2III)	HD 78479 (K3III)	Δ_a (per cent)	Δ_b (per cent)
10	24.7	25.6	5.9	3.8	10.9	3.4	4.0	17.4	19.4	–	–
20	32.3	33.2	23.5	20.0	24.2	22.8	22.2	23.4	24.8	66	24
30	40.9	42.2	33.4	30.0	33.8	32.4	32.2	33.7	35.3	41	18
40	51.1	52.3	43.7	40.0	44.0	43.0	42.6	44.2	46.8	31	17
50	62.4	63.7	54.3	50.0	54.7	53.7	52.9	54.7	57.5	27	15
60	73.8	75.1	64.9	60.0	65.7	64.0	63.6	65.1	67.4	25	12
70	84.8	86.1	74.5	70.0	76.5	74.4	73.8	75.2	77.0	23	10
80	95.4	96.8	84.7	80.0	87.0	84.4	84.0	85.5	86.8	21	9
90	105.9	107.5	94.8	90.0	97.3	94.3	93.9	95.4	96.9	19	8
100	116.4	118.3	105.4	100.0	107.5	104.8	103.9	105.7	106.7	18	8
110	127.0	129.1	115.8	110.0	117.7	115.2	114.1	115.8	116.7	17	7
120	137.6	140.0	125.7	120.0	128.0	125.1	124.1	126.3	126.4	17	7
130	148.4	150.9	136.5	130.0	138.2	135.6	134.2	136.2	136.2	16	6
140	159.2	161.9	147.1	140.0	148.5	146.2	144.0	146.6	146.1	16	6

spectra in all panels of Fig. 7 using Set80. For panels of Fig. 7, from top to bottom, the results are $\sigma_m = 10.5 \pm 2.3, 29.7 \pm 1.3, 49.8 \pm 1.3, 79.5 \pm 1.9$ and 99.3 ± 2.5 km s^{-1}, respectively. As expected, there is no significant offset from the input velocity dispersion when we use the mixed stellar templates.

4.3 Best-fitting error analysis

In addition to the above, we repeated the same analysis for each galaxy to construct an ensemble of simulated spectra by adding the corresponding random noise to the best fits provided by PPXF (e.g. red curve in Fig. 2). This technique effectively gives the statistical errors of both measured radial velocity and velocity dispersion. In the case of having few templates (e.g. when using Set50 or Set80), this

method is applied with the use of the equivalent synthetic template based on the best output weights. Applying the multiple stellar templates reduces the effect of the template mismatch particularly when dealing with low S/N spectra of faint galaxies which are expected to have smaller mass and internal velocity dispersion.

4.4 The catalogue uncertainties

All the stellar templates in Table 2 were used to measure velocity dispersions for each galaxy in our sample. We used the rms scatter around the mean values as the likely template mismatch uncertainty (see column 9 of Table 6). Since the exact combination of the stellar templates is unknown for each galaxy, the exact value of the template mismatch uncertainty depends on the selected templates

Table 6. Radial velocity, V_r, and velocity dispersion, σ, of dwarf galaxies in our sample. In columns 11 and 12, we have a list of common galaxies in the literature and their σ. In column 12, the data denoted by asterisks are from MLKC02 and the rest are from Co09. The likely errors in measured σ due to the effect of template mismatch are illustrated in column 9. The statistical uncertainties in σ are listed in column 10. Column 8 shows the final uncertainty of σ for all uncertainty sources and is obtained by adding columns 9 and 10 in quadrature. Column 13 is the S/N of the galaxy spectra which are calculated per pixel (0.33 Å). Column 14 shows the number of stellar templates used to describe the galaxy spectra in the Set80 run.

GMP ID (1)	RA (J2000) (2)	Dec. (J2000) (3)	R_{SDSS} (mag) (4)	cz (km s^{-1}) (5)	δcz (km s^{-1}) (6)	σ (km s^{-1}) (7)	$\Delta\sigma$ (km s^{-1}) (8)	$\delta\sigma_1$ (km s^{-1}) (9)	$\delta\sigma_2$ (km s^{-1}) (10)	σ(MG05) (km s^{-1}) (11)	σ(Literature) (km s^{-1}) (12)	S/N 1/pixel (13)	# of Temperature (14)
3534	12:59:21.40	27:58:24.80	16.13	6001	7	30	7	7	3	53 ± 3	$65 \pm 6^*$	45	7
3474	12:59:26.40	27:59:18.30	18.69	7666	6	22	4	3	2	–	–	37	5
3471	12:59:26.60	27:59:54.50	15.35	6624	13	79	5	5	2	86 ± 3	$85 \pm 8^*$	80	7
3438	12:59:28.50	28:01:09.40	18.05	5952	31	26	8	7	3	32 ± 11	–	16	3
3424	12:59:29.30	27:56:32.00	18.27	5596	7	27	9	7	5	–	–	29	6
3406	12:59:30.30	28:01:15.10	17.41	7116	7	36	3	2	2	–	–	29	3
3376	12:59:32.10	27:55:15.80	17.25	7004	22	37	3	3	2	–	28 ± 4	19	5
3340	12:59:35.20	27:56:05.00	17.73	4476	12	43	8	6	5	–	–	17	2
3336	12:59:35.50	27:54:21.60	17.61	6954	6	42	4	4	2	52 ± 5	–	47	5
3325	12:59:36.00	27:54:22.00	17.58	8953	13	38	7	6	2	–	–	18	2
3312	12:59:37.00	28:01:07.00	17.42	7156	27	31	4	3	2	85 ± 3	–	44	5
3308	12:59:37.20	27:58:19.90	18.09	7522	8	50	4	3	2	–	–	57	4
3296	12:59:37.90	27:54:26.40	14.3	7948	21	178	7	5	4	179 ± 4	$180 \pm 4^*$	87	1
3292	12:59:38.00	28:00:03.70	16.25	4951	8	40	5	3	3	63 ± 6	–	48	5
3223	12:59:42.40	28:01:58.60	18.41	7797	16	22	9	8	5	–	–	11	3
3209	12:59:44.20	28:00:47.00	18.58	7111	17	30	5	4	2	66 ± 14	–	30	5
3166	12:59:46.90	27:59:30.90	17.39	8292	7	38	6	6	3	58 ± 8	35 ± 4	26	4
3146	12:59:48.60	27:58:58.00	17.74	5358	10	38	11	9	6	–	–	11	3
3141	12:59:49.10	27:58:33.90	19.86	4957	26	59	15	11	10	–	–	5	2
3131	12:59:50.20	27:54:45.50	17.29	7183	14	19	7	6	4	–	–	22	4
3119	12:59:51.50	27:59:35.50	19.74	7060	14	37	10	9	5	–	–	8	3
3098	12:59:53.90	27:58:13.70	17.73	6740	8	33	7	5	5	–	–	28	5
3080	12:59:55.70	27:55:03.80	18.11	6599	10	9	8	6	5	–	16 ± 4	19	5
3018	13:00:01.00	27:59:29.60	18.17	7464	10	38	5	5	3	–	–	15	3
2983	13:00:04.00	28:00:30.70	19.03	6349	10	27	6	5	3	–	–	18	3
2960	13:00:05.40	28:01:28.00	15.18	5866	7	60	5	5	3	68 ± 2	$64 \pm 5^*$	62	5
2931	13:00:07.10	27:55:51.50	17.59	7704	17	35	6	4	4	–	–	47	5
2877	13:00:11.40	27:54:36.40	18.71	7225	12	29	9	8	5	–	–	14	5
2839	13:00:14.70	28:02:26.90	14.43	5706	15	168	6	5	3	160 ± 3	–	57	4
2808	13:00:17.00	27:54:16.10	19.64	8944	16	69	12	9	8	–	–	13	2
2780	13:00:18.70	27:55:12.70	19.06	6554	18	63	12	9	8	–	–	13	2
2755	13:00:20.20	27:59:37.60	18.87	6812	13	27	9	8	4	–	–	14	2
2736	13:00:21.70	27:53:54.80	16.41	4857	5	35	4	3	2	–	35 ± 3	42	4
2718	13:00:22.70	27:57:55.00	18.76	6360	12	30	8	7	4	–	–	13	4
2676	13:00:26.20	28:00:32.00	17.86	5516	30	37	8	7	4	–	–	19	4
2655	13:00:27.90	27:59:16.50	19.46	9412	14	45	5	5	2	–	–	12	3
2654	13:00:28.00	27:57:21.60	14.87	7009	21	144	7	6	3	-142 ± 4	–	66	3
2605	13:00:33.30	27:58:49.40	18.28	5126	12	36	10	8	6	–	–	13	3
2591	13:00:34.40	27:56:05.00	17.17	8653	14	53	9	8	4	–	–	20	2
2571	13:00:36.60	27:55:52.20	18.68	5944	18	17	6	5	3	–	–	20	3
2563	13:00:37.30	27:54:41.10	19.5	5895	11	25	10	9	5	–	–	9	2

for measurements. Even though Table 2 covers various metallicities and spectral types, choosing another set of templates may slightly alter this estimate, due to the multistellarity of galaxies. For 66 per cent of the galaxies in Table 6, the mismatch error is estimated to be less than 20 per cent and only exceeds 25 per cent for 22 per cent of the galaxies. The average template mismatch errors are 4, 12 and 18 per cent for galaxies with the measured velocity dispersions greater than $100\,\mathrm{km\,s^{-1}}$, between 50 and $100\,\mathrm{km\,s^{-1}}$ and between 20 and $50\,\mathrm{km\,s^{-1}}$, respectively. These results which are purely obtained from observation are consistent with those estimated using simulations described in Section 4.2. Fig. 5 shows that the mismatch effect decreases as the velocity dispersion increases. Simulations indicate that the average uncertainty due to the template mismatch is about

15 per cent for $\sigma \sim 50\,\mathrm{km\,s^{-1}}$ and ~ 5 per cent for $\sigma \gtrsim 100\,\mathrm{km\,s^{-1}}$, which is consistent with the reported values in column 9 of Table 6.

In Section 3, it is mentioned that using Set50 improves the χ^2 by ~ 10 per cent on average, while adding 30 more templates reduces the χ^2 by only ~ 1 per cent on average. Hence, a larger number of templates were not considered due to their very limited effect. Since the reported σ is based on Set80 and the corresponding statistical uncertainty (see Section 4.3) is not very different from that of the individual template analysis (see Section 4.1), we obtained the statistical uncertainties for each sample galaxy by applying the method described in Sections 4.1 and 4.3 for Set80 (see column 10 of Table 6). Assuming that the use of Set80 eliminates the mismatch effect (see Section 4.2), one can take these values as the final
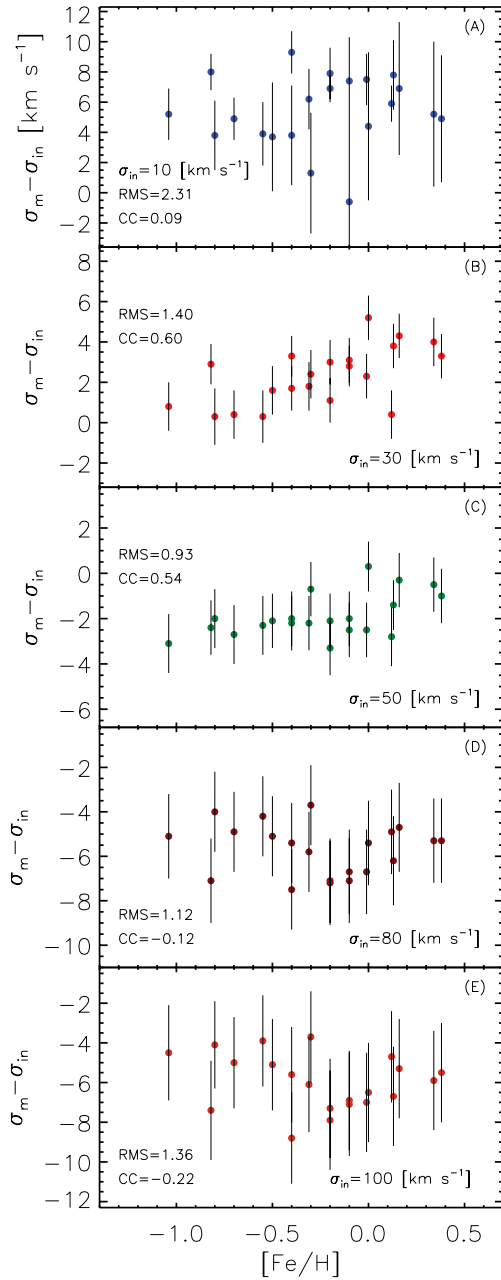
Figure 7. The difference between the measured velocity dispersion, σ_m, and the given input velocity dispersion, σ_{in}, against the metallicity, [Fe/H], of the templates used for measurements. We used the star spectrum HD 45282, observed by DEIMOS, as the input spectrum. In each panel, this spectrum was broadened according to the range of input velocity dispersions. For all simulated spectra, S/N = 30. In each case, the error bar is calculated based on 300 simulations. For measurements, we used several templates from the Indo-US library with the same spectral type (i.e. G8III) and metallicities ranging between −1 and 0.4 (in solar units). In each panel, RMS is the root mean square of the difference between the input and the measured velocity dispersions, and CC shows the coefficient of the correlation between $\sigma_m - \sigma_{in}$ and the metallicity of the templates used for measurements. As seen, the measured velocity dispersions are independent of the metallicity within ∼ 2 km s^{-1} uncertainty for σ_{in} > 10 km s^{-1}.
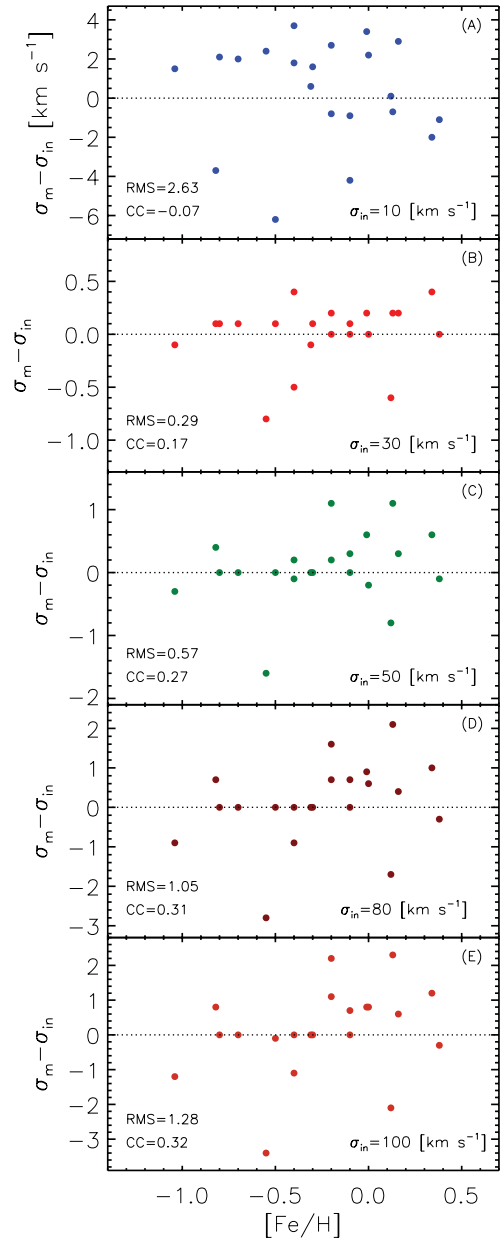
Figure 8. Same as Fig. 7 except for the templates used for simulations and measurements. To perform the simulation, we used several templates from the Indo-US library with the same spectral type (i.e. G8III) and metallicities ranging between −1 and 0.4. In each panel, the templates were broadened according to the desired input velocity dispersions. In this level of simulations, no noise was added to the simulated spectra. For measurements, we used the Set80 templates. As seen, when using Set80, the measured velocity dispersions are the same as the input velocity dispersions within ∼2 km s^{-1} uncertainty for σ_{in} > 10 km s^{-1}. In each panel, RMS is the root mean square of the difference between the input and the measured velocity dispersions, and CC denotes the coefficient of the correlation between $\sigma_m - \sigma_{in}$ and the metallicity of the templates used for measurements. No significant correlation is seen between the measured and input velocity dispersions when we use Set80. To avoid any confusion, the error bars are not shown in this diagram. Here, the typical uncertainty in measured velocity dispersions is ∼2 km s^{-1}.

uncertainty of the measured velocity dispersions. Being more conservative, in column 8 of Table 6, we derived the final error of the measured σ as the quadratic combination of both uncertainties (columns 10 and 11). These values are used for further analysis in this paper and Paper II (Kourkchi et al. 2012).

We performed the same analysis to obtain the uncertainty of the measured radial velocities. The effect of the template mismatch on measured radial velocities is less than 1 per cent, because this measurement is only sensitive to the exact location of the absorption lines of the applied stellar templates which are slightly altered from one template to another. The final radial velocities and their corresponding uncertainties are obtained based on the Set80 run (columns 5 and 6 of Table 6).

5 RESULTS AND DISCUSSION

We present the radial velocities, V_r, and velocity dispersions, σ, of 41 dwarf elliptical galaxies in the Coma cluster in Table 6. Of these galaxies, 12 have S/N < 15 pixel^{-1} in their spectra. The reported values are measured based on Set80, as explained in Section 3.

Figure 9. Radial velocities from MG05 (open circles), MLKC02 (filled diamonds) and Co09 (red stars) versus velocities in this study. The dotted line shows equality indicating that the velocities of MLKC02 and Co09 are systematically greater.
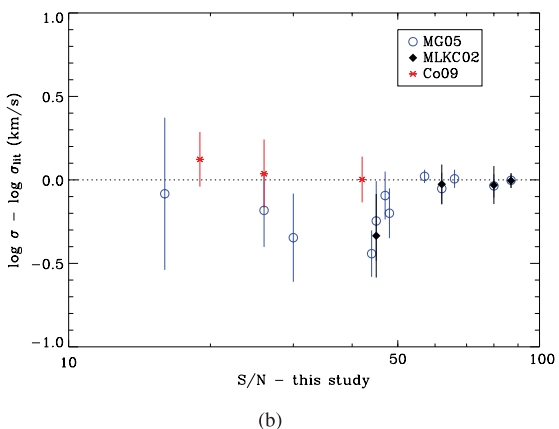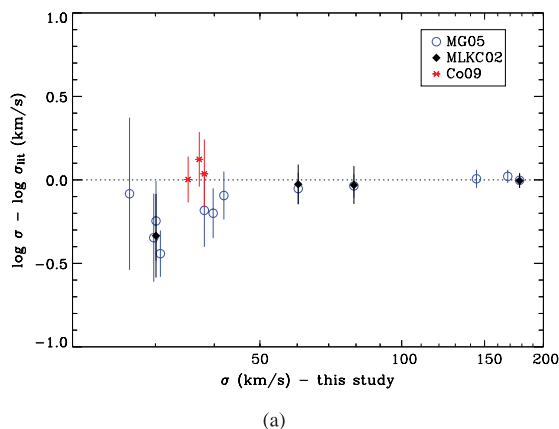
We compare our measured V_r and σ values with MG05, MLKC02 and Co09 in Figs 9 and 10. The mean difference between our V_r values and those of MG05 is $\sim$8 km s^{-1}. However, when we include the V_r measurements from Co09, the mean difference is $\sim$20 km s^{-1}. Comparison of the velocity dispersion with MG05 (see Fig. 10) shows that for smaller values of velocity dispersion (i.e. σ < 50 km s^{-1}), our values are relatively smaller. Such discrepancy is likely due to the different methods of measurement, and/or to different templates used for measurement and/or to different wavelength regimes used for analysis. Since CaT lines are more prominent in dE galaxies than the absorption lines in the wavelength range $\sim$4200–5700 Å, as used in the studies of MG05 and Co09, our measurements of V_r and σ are more robust. Our analysis also includes measurements with 80 mixed stellar templates and detailed analysis of the uncertainties.

In addition, of 41 studied galaxies in this paper, 12 galaxies were observed twice using two different masks. In Table 7, for each

Table 7. The measured velocity dispersion of the galaxies which were observed with two different masks. Columns 2 to 5 are the mask IDs also presented in Table 1. For these galaxies, we added both spectra of two masks to get the larger S/N values. In the last column, the measured velocity dispersion of the added spectra is presented. The velocity dispersions are in terms of km s^{-1} and the errors are based on the statistical uncertainties. As seen, the measured velocity dispersions for each galaxy are consistent within the error bars.

GMP	Coma1-1	Coma1-2	Coma2-1	Coma2-2	Add
3424	–	–	27 ± 7	26 ± 7	27 ± 5
3223	16 ± 9	29 ± 8	–	–	22 ± 5
3209	32 ± 3	29 ± 5	–	–	30 ± 2
3119	40 ± 7	32 ± 7	–	–	37 ± 5
3080	–	–	8 ± 9	13 ± 9	9 ± 5
2983	23 ± 6	28 ± 5	–	–	27 ± 3
2877	–	–	32 ± 8	30 ± 7	29 ± 5
2808	–	–	75 ± 11	71 ± 9	69 ± 8
2755	22 ± 6	31 ± 7	–	–	27 ± 4
2718	–	–	33 ± 5	29 ± 6	30 ± 4
2605	41 ± 9	32 ± 8	–	–	36 ± 6
2571	–	–	17 ± 4	14 ± 4	17 ± 3

(a)   (b)

Figure 10. The differences in measured velocity dispersion in this study and common galaxies in the literature (MG05, MLKC02 and Co09) are plotted against our measured velocity dispersion and S/N value in the left- and right-hand panels, respectively. To derive 1σ errors, the errors of our σ measurement and those from the literature are added in quadrature. The horizontal axis is logarithmically scaled. As seen, except for four measured values, the rest are consistent with the literature within the error bars. There is a good consistency for σ > 50 km s^{-1} for which $\langle\sigma/\sigma_{lit}\rangle$ is 0.97 ± 0.05 and for σ < 50 km s^{-1} for which $\langle\sigma/\sigma_{lit}\rangle$ is 0.97 ± 0.17.

of these galaxies we compare the measured velocity dispersions using both observed spectra. We also added both spectra of these galaxies to get better S/N and then repeated the measurements. As seen, considering the statistical uncertainties, the measurements are consistent.

5.1 Faber–Jackson relation

The relation between luminosity and velocity dispersion of bright elliptical galaxies was originally discovered by Faber & Jackson (1976) and is expressed as $L \propto \sigma^\alpha$. For brighter ellipticals α is ∼4 while fainter galaxies exhibit a shallower slope. Davies et al. (1983) were the first to note that α changes from ∼4 to ∼2.4, for elliptical galaxies fainter than $M_R \simeq 21.7$ mag. This result was also confirmed by Held et al. (1992) who found $\alpha = 2.5$ for dE galaxies. These results were finally extended to lower luminosities by MG05 and Co09 who found $\alpha \simeq 2.0$. In this paper, we present data for 26 dE galaxies in the Coma cluster down to $M_R \simeq -15$ mag. Using the orthogonal distance regression, we derive the FJ relation to be $L \propto \sigma^{2.34\pm0.19}$ for the entire sample, and $L \propto \sigma^{1.99\pm0.14}$ for galaxies brighter than $M_R \simeq -16$ mag.

We show the L–σ relation for the galaxies in our sample in Figs 11 and 12, where we also include the sample of Co09 and MG05. We excluded the spiral galaxies from Co09 when deriving the FJ relation. The L–σ correlation coefficient is −83 per cent at a significance of 99.99 per cent (i.e. only a 0.01 per cent chance that the correlation is due to the random scatter). We perform linear fits via two methods, the least-squares bisector fit and the orthogonal distance regression. Both methods incorporate the errors in our measurements and those reported in the literature. In orthogonal distance regression, the orthogonal distance of data points from the line is minimized. The magnitudes of all galaxies in Fig. 11 and the left-hand panel of Fig. 12 are derived from SDSS DR7. To transform SDSS *ugriz* magnitudes into the Johnson–Cousins

Figure 11. The FJ relation for three samples of dwarf galaxies in the Coma cluster. The filled black diamonds represent the dwarf elliptical sample from DEIMOS/Keck observations. The red asterisks are dEs from C09 and the green open circles are data from MG05. Except for one point, the DEIMOS sample provides the only measurements at $M_R \geq -16$. The dashed line is the least-squares orthogonal distance fit for DEIMOS+MG05 data while the dash–dotted line is the best orthogonal fit for all three samples. Of our sample, six of the faintest galaxies are labelled with their GMP IDs. The dotted line shows the least-squares orthogonal fit excluding the six galaxies fainter than $M_R = -16$ mag. See Table 8 for detailed results.

R magnitude, we used the mean value of the following relations presented on the SDSS DR6 website.[2]

$$R = r - 0.1837 \times (g - r) - 0.0971, \tag{3}$$

$$R = r - 0.2936 \times (r - i) - 0.1439. \tag{4}$$

The results of the least-squares fit are available in Table 8. We ran the same analysis for the same sample using the Canada–France–Hawaii Telescope (CFHT) Megacam *i*-band data. We find that our FJ relation slope is consistent with those of Co09 and MG05 within the errors, for both linear fitting methods. The least-squares bisector method yields $L_R \propto \sigma^{1.94\pm0.16}$, while we derive $L_R \propto \sigma^{2.34\pm0.19}$ via the orthogonal regression method. Using the CFHT *i*-band data, the best fits of the FJ relation are consistent with those derived from SDSS data (see Table 8). The behaviour at the faint end of the FJ relation is uncertain as many of our galaxies in this magnitude range ($M_R > -16$) have S/N < 15 pixel^{-1}. However, our results imply that the slope of the FJ relation may change towards higher velocity dispersions at this faint end. Excluding galaxies fainter than $M_R \simeq -16$, FJ is $L_R \propto \sigma^{1.99\pm0.14}$.

Next, we use photometry from the *HST*/ACS Coma Treasury Survey (Carter et al. 2008) to derive the FJ relation. Out of 41 galaxies in our sample, 28 have available *HST*/ACS magnitudes, together with 43 galaxies from the MG05 and Co09 samples. In Fig. 12 and Table 8, we show the best linear fits of the FJ relation using *HST*/ACS *F814W* (*I* band) and *F475W* (*g* band). We find that the FJ relation shows no discrepancy in colour.

Following all the above analysis, we noted that for one of our sample galaxies (GMP 3308), the SDSS magnitudes are almost one magnitude fainter than what is derived from CFHT and *HST* images. Therefore, we modified the SDSS R magnitude of this galaxy by constructing a linear trend between the CFHT *i* band and SDSS R magnitudes of all sample galaxies.

5.2 Colour–σ relation

The relation between the dynamical mass of galaxies and their stellar population can be studied using the colour–σ diagram. MG05 showed a well-defined colour–σ relation for faint early-type galaxies brighter than $M_R = -17.5$ mag. In panel (A) of Fig. 13, we extend the relation to fainter dEs ($M_R < -15$ mag) which are located at the blue end of the diagram and are more scattered around the the fitted line for brighter galaxies [i.e. for $M_R > -17$ mag the relation is $B - R = (0.23\pm0.03)\log\sigma + (1.02\pm0.23)$]. The scatter of dEs around the colour–σ relation could be due to their different formation history, age and metallicity. To calculate the colour of the galaxies, $B - R$, we used the SDSS data and the transformation functions presented on the SDSS website to derive the Johnson B and R magnitudes. Panel (B) of Fig. 13 shows the same relation using $m_{475} - m_{814}$ colour of the galaxies in the *HST*/ACS field.

The dependence of the internal velocity dispersion of dEs and their central activity is investigated in panel (C) of Fig. 13. Central colours of the galaxies for which we have the *HST*/ACS images are calculated within the aperture with a diameter of 0.4 arcsec (i.e. 185 pc at the location of the Coma cluster). We found a linear trend between the velocity dispersion of dEs and their central colours, except for very faint galaxies which have bluer cores, ($m_{475} - m_{814}$) < 1.0.
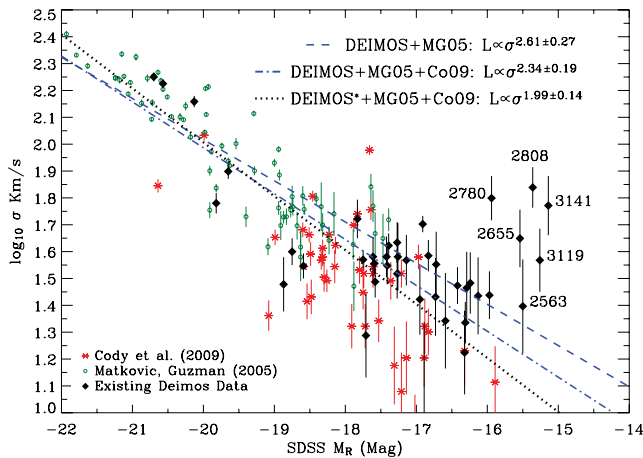
[2] http://www.sdss.org/dr6/algorithms/sdssUBVRITransform.html, see also Jordi, Grebel & Ammon (2006) and Ivezić et al. (2007).
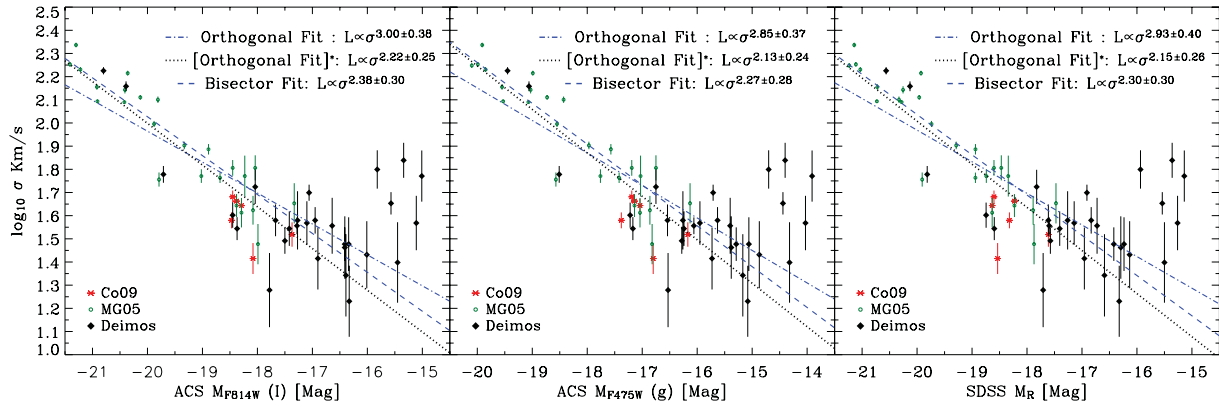
Figure 12. Same as Fig. 11. The FJ relation for three samples of dwarf galaxies which lie in the footprint of the *HST*/ACS Coma Treasury Survey (Carter et al. 2008). The left-hand panel shows the FJ relation for this sample using magnitudes based on SDSS data. For the left-hand and middle panels, magnitudes are derived from the Treasury *HST*/ACS images in the *F814W* (*I* band) and *F475W* (*g*-band) filters (Paper II). The dashed line is the least-squares bisector fit, and the dash–dotted line is obtained using the orthogonal distance regression. The dotted line shows the orthogonal fit for galaxies brighter than $M_R = -16$ mag. We see no colour dependence of the FJ within the error bars.

Table 8. Least-squares fit to find the L–σ relation. (1) The sample galaxies used in regression. (2) Survey filters for the magnitude of the sample galaxies. (3) The order of regression. For example, in the first row residuals in $\log \sigma$ are minimized. (4) and (5) The slope and intercept of $M = A\log \sigma + B$ and their 1σ uncertainties. (6) α in the FJ relation ($L \propto \sigma^\alpha$). We have used the data with S/N > 15 Å^{-1} of MG05 and all dEs of Co09.

Sample galaxies (1)	Filter (2)	Regression (3)	Slope (A) (4)	Intercept (B) (5)	α (6)
DEIMOS+MG05	SDSS *R*	$\log \sigma$	-6.59 ± 0.67	-6.72 ± 2.17	2.64 ± 0.27
DEIMOS+MG05	SDSS *R*	M_R	-4.55 ± 0.38	-10.45 ± 0.76	1.81 ± 0.15
DEIMOS+MG05	SDSS *R*	Bisector	-5.57 ± 0.55	-8.59 ± 1.63	2.23 ± 0.22
DEIMOS+MG05	SDSS *R*	Orthogonal	-6.52 ± 0.67	-6.84 ± 2.19	2.61 ± 0.27
DEIMOS*+MG05	SDSS *R*	Orthogonal	-5.41 ± 0.49	-9.02 ± 2.02	2.16 ± 0.20
DEIMOS+MG05+Co09	SDSS *R*	Bisector	-4.85 ± 0.40	-10.12 ± 1.31	1.94 ± 0.16
DEIMOS+MG05+Co09	SDSS *R*	Orthogonal	-5.85 ± 0.49	-8.37 ± 1.79	2.34 ± 0.19
DEIMOS*+MG05+Co09	SDSS *R*	Orthogonal	-4.98 ± 0.35	-10.00 ± 1.58	1.99 ± 0.14
DEIMOS+MG05+Co09	CFHTLS *i*	Bisector	-4.73 ± 0.38	-10.33 ± 1.27	1.89 ± 0.15
DEIMOS+MG05+Co09	CFHTLS *i*	Orthogonal	-5.61 ± 0.45	-8.81 ± 1.73	2.25 ± 0.18
DEIMOS*+MG05+Co09	CFHTLS *i*	Orthogonal	-4.82 ± 0.33	-10.29 ± 1.54	1.93 ± 0.13
[DEIMOS*+MG05+Co09]	*HST*/ACS *F814W* (*I*)	Orthogonal	-5.55 ± 0.63	-8.90 ± 2.49	2.22 ± 0.25
[DEIMOS*+MG05+Co09]	*HST*/ACS *F475W* (*g*)	Orthogonal	-5.33 ± 0.61	-8.02 ± 2.35	2.13 ± 0.24
[DEIMOS*+MG05+Co09]	SDSS *R*	Orthogonal	-5.37 ± 0.64	-9.21 ± 2.64	2.15 ± 0.26

All galaxies in the [DEIMOS+MG05+Co09] sample have *HST*/ACS data. DEIMOS* represents the DEIMOS sample excluding galaxies fainter than $M_R = -16$ mag.

5.3 Remarks on faint galaxies

Of six faintest galaxies from the DEIMOS sample, GMP 2808, GMP 2655, GMP 3119, GMP 2780 and GMP 3141 are bluer than all other sample galaxies (see Fig. 13) and have larger velocity dispersion with respect to the L–σ relation of brighter galaxies (see Fig. 8).

In order to test the effect of stellar population on measured velocity dispersions, we have repeated the σ measurement using two sets of stellar templates. The first set consists of 10 F stars with different spectral types and metallicities (hereafter F-lib). The second set includes both F-lib and the G/K stars of Table 3 (hereafter FGK-lib). The results of σ measurements based on Set80, FGK-lib and F-lib are compared in Table 9. The analysis based on FGK-lib shows no changes in results except for GMP 2808 which is the bluest galaxy in our sample. The measured σ of GMP 3119 and GMP 2808 in

the F-lib run is smaller than those of the Set80 and FGK-lib runs; however, the resulting χ^2 is higher for the F-lib run. The maximum change in measured σ for all other galaxies in our sample in the FGK-lib run is less than 2 km s^{-1}. As a result, the measured σ values in Table 6 are independent of the stellar population except for the bluest galaxy, for which blue stellar templates should be used for σ measurement.

Recent gas-rich mergers in blue dEs may be responsible for their deviation from the FJ relation. Supernova-driven winds can expel the luminous matter of these galaxies and shift them to the faint end of the FJ diagram. Moreover, the resulting starburst due to the inward gas transportation during the merger produces the central excess light compared to the extrapolated Sérsic function of the galaxy's outer region (Kormendy et al. 2009). The correlation between the central extra light and deviation of faint dEs from the scaling relations of brighter ellipticals is studied in Paper II.
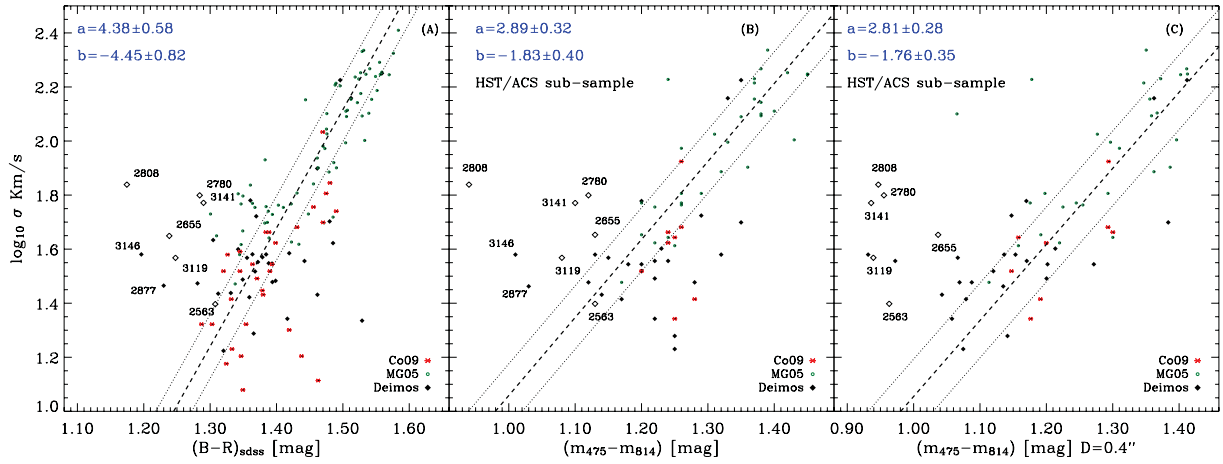
Figure 13. Colour–σ relation for three samples of dwarf ellipticals in the Coma cluster. The filled black diamonds represent dEs from our DEIMOS/Keck sample. The open diamonds represent faintest dEs of our sample which are labelled with their GMP IDs. The red asterisks are dEs from Co09 and the green open circles are from MG05. The dashed line shows the best linear orthogonal fit for brighter galaxies, $M_R > -17$ mag, and the dash–dotted lines represent 1σ uncertainty along the vertical axis. In all panels, a and b are the slope and intercept of the fitted lines, respectively. Panel (A) shows the colour–σ relation using the magnitudes from SDSS DR7. Panel (B) shows the colour–σ relation for a subsample of dEs for which their *HST*/ACS magnitudes in *F475W* (*g*) and *F814W* (*I*) bands are available. Panel (C) is the same as panel (B) except for the colour of galaxies which are calculated within the aperture with diameter of 0.4 arcsec (i.e. 185 pc at the location of the Coma cluster).

Table 9. The results of σ measurements for eight blue galaxies based on different template libraries.

GMP ID	σ (km s^{-1}) Set80	FGK-lib	F-lib
3146	38	37	35
3141	59	60	61
3119	37	35	26
2877	29	27	26
2808	69	39	38
2780	63	63	31
2655	45	45	42
2563	25	25	28

6 SUMMARY

We have observed a sample of $\sim$50 dwarf elliptical galaxies in the core of the Coma cluster of which we measured the internal velocity dispersions for 41 dwarfs. For 26 galaxies, we presented the velocity dispersion for the first time. Our current study extends the relation 1 mag fainter than previous studies in Coma. We performed a comprehensive analysis to find the source of the uncertainties when measuring the velocity dispersion. We found that the main uncertainty may arise due to the mismatch of the stellar templates. This kind of uncertainty is less than 20 per cent of the measured velocity dispersion for $\sigma \sim 50$ km s^{-1}. The template mismatch uncertainty decreases for higher velocity dispersions and is reduced to $\sim$5 per cent for $\sigma \gtrsim 100$ km s^{-1}. We find greater velocity dispersions when using templates with lower stellar metallicities. The effect of template mismatch is reduced with the use of multiple stellar templates and the optimization of the template weights to reproduce each sample galaxy spectrum. In addition, using the multiple stellar templates removes the dependence of the measurements on galaxy and/or templates metallicity. Casting our data points and those from the literature, we get the L–σ relation as $L \propto \sigma^{1.99 \pm 0.14}$. We noted that fainter dwarfs show a departure from the FJ relation of the brighter ellipticals, which indicates that they

have a higher velocity dispersion than what is predicted by the L–σ linear trend. In Paper II, we will present the combined study of the photometric and spectroscopic properties of this sample, focusing on the Fundamental and the Photometric Plane of the galaxies.

REFERENCES

Aaronson M., 1983, ApJ, 266, L11
Adami C. et al., 2006, A&A, 451, 1159
Bender R., Burstein D., Faber S. M., 1992, ApJ, 399, 462
Cappellari M., Emsellem E., 2004, PASP, 116, 138
Carrera R., Gallart C., Pancino E., Zinn R., 2007, AJ, 134, 298
Carter D. et al., 2008, ApJS, 176, 424
Cenarro A. J., Gorgas J., Vazdekis A., Cardiel N., Peletier R. F., 2003, MNRAS, 339, 12
Cody A. M., Carter D., Bridges T. J., Mobasher B., Poggianti B. M., 2009, MNRAS, 396, 1647 (Co09)
Davies R. L., Efstathiou G., Fall M., Illingworth G., Schechter R. L., 1983, AJ, 266, 41
Davis M. et al., 2003, in Guhathakurta P., ed., Proc. SPIE Vol. 4834, Discoveries and Research Prospects from 6- to 10-Meter-Class Telescopes II. SPIE, Bellingham, p. 161

De Rijcke S., Prugniel P., Simien F., Dejonghe H., 2006, MNRAS, 369, 1321

Dekel A., Silk J., 1986, ApJ, 303, 39

Díaz A. I., Terlevich E., Terlevich R., 1989, MNRAS, 239, 325

Djorgovski S., Davis M., 1987, ApJ, 313, 59

Dressler A., Lynden Bell D., Burstein D., Davies R. L., Faber S. M., Terlevich R., Wegner G., 1987, ApJ, 313, 42

Faber S. M., Jackson R. E., 1976, ApJ, 204, 668

Faber S. M. et al., 2003, in Iye M., Moorwood F. M., eds, Proc. SPIE Vol. 4841, Instrument Design and Performance for Optical/Infrared Ground-Based Telescopes. SPIE, Bellingham, p. 1657

Foster C., Forbes D. A., Proctor R. N., Strader J., Brodie J. P., Spitler L. R., 2010, AJ, 139, 1566

Geha M., Guhathakurta P., van der Marel R. P., 2002, AJ, 124, 3073

Godwin J. G., Metcalfe N., Peach J. V., 1983, MNRAS, 202, 113

Graham A. W., Guzmán R., 2003, AJ, 125, 2936

Held E. V., de Zeeuw T., Mould J., Picard A., 1992, AJ, 103, 851

Ivezić Ž. et al., 2007, in Sterken C., ed., ASP Conf. Ser. Vol. 364, The Future of Photometric, Spectrophotometric and Polarimetric Standardization. Astron. Soc. Pac., San Francisco, p. 165

Jordi K., Grebel E. K., Ammon K., 2006, A&A, 460, 339

Jørgensen U. G., Carlsson M., Johnson H. R., 1992, A&A, 254, 258

Jørgensen I., Franx M., Kjaergaard P., 1996, MNRAS, 280, 167

Kormendy J., Fisher D. B., Cornell M. E., Bender R., 2009, ApJS, 182, 216

Kourkchi E., Khosroshahi H. G., Carter D., Mobasher B., 2012, MNRAS, in press (doi:10.1111/j.1365-2966.2011.19980.x)

Lejeune Th., Cuisinier F., Buser R., 1997, A&AS, 125, 229

Mallik S. V., 1994, A&AS, 103, 279

Mateo M., 1998, ARA&A, 36, 435

Matković A., Guzmán R., 2005, MNRAS, 362, 289 (MG05)

Michielsen D. et al., 2007, ApJ, 670, 101

Moore S. A. W., Lucey J. R., Kuntschner H., Colless M., 2002, MNRAS, 336, 382 (MLKC02)

Pritchet C., 1978, ApJ, 221, 507

Schulz J., Fritze-v. Alvensleben U., Móller C. S., Fricke K. J., 2002, A&A, 392, 1

Smith G., Drake J. J., 1990, A&A, 231, 125

Starkenburg E. et al., 2010, A&A, 513, A34

Toloba E., Boselli A., Cenarro A. J., Peletier R. F., Gorgas J., Gil de Paz A., Muñoz-Mateos J. C., 2011, A&A, 526, 114

Tonry J., Davis M., 1979, AJ, 84, 1511

Valdes F., Gupta R., Rose J. A., Singh H. P., Bell D. J., 2004, ApJS, 152, 251

Yoshii Y., Arimoto N., 1987, A&A, 188, 13

Zhou X., 1991, A&A, 248, 367

This paper has been typeset from a TEX/LATEX file prepared by the author.